XLVI CILAMCE
VITÓRIA - ES - BRAZIL - 2025
XLVI IBERO-LATIN AMERICAN CONGRESS ON COMPUTATIONAL METHODS IN ENGINEERING

Aeroelastic analysis of spoilers on low-rise buildings using a finite element model for fluid-structure interaction

Gabriela P. Bianchin[1], Renato V. Linn[2], Alexandre L. Braun[2]

[1]*PhD. Student. Programa de Pós-Graduação em Eng. Civil, Universidade Federal do Rio Grande do Sul*
Av. Osvaldo Aranha, 99, 90035-190, Porto Alegre/Rio Grande do Sul, Brasil
pbianchingabi@gmail.com
[2]*Professor, Programa de Pós-Graduação em Eng. Civil, Universidade Federal do Rio Grande do Sul*
Av. Osvaldo Aranha, 99, 90035-190, Porto Alegre/Rio Grande do Sul, Brasil
renatolinn@ufrgs.br; alexandre.braun@ufrgs.br

Abstract. Low-rise buildings are highly susceptible to wind action due to the development of high suction pressures on their roofs, which result from vortices generated near the roof's corners and edges. To mitigate wind loads on the roof structure, aerodynamic appendages may be incorporated into the building design. Previous work (Bianchin and Braun [1]) has shown that rigid spoilers can effectively reduce aerodynamic loading on the roofs of low-rise buildings. However, the feasibility of this load mitigation method depends on the spoiler dynamic stability and the strain/stress levels developed in the spoiler material. In this context, a fluid-structure interaction (FSI) model is proposed to numerically investigate the aeroelastic behavior and stress states induced by wind on aerodynamic appendages that are intended for future use in low-rise buildings to attenuate aerodynamic loading on roofs. In the present model, spoilers are considered elastic structures constituted of linear elastic material with geometrically nonlinear effects. Results obtained here are compared with previous predictions using rigid spoilers. This study demonstrates the feasibility of using aerodynamic appendages for wind load attenuation in buildings, provided that they are not subject to excessive loading or aeroelastic phenomena.

Keywords: computational wind engineering (CWE), fluid-structure interaction (FSI), spoilers, aeroelasticity, nonlinear structures.

1 Introduction

Low-rise building roofs are known to be susceptible to the wind action due to strong pressure loads developed over the roof surfaces, which are induced by flow separation occurring at roof sharp edges, such as eaves and ridges, especially under extreme climate events. It is also well known that the failure mechanism of structural and covering elements localized in the roof are intimately related to load resultants obtained from the combination of inner and outer pressure conditions, where wall openings play a major role. Among several pressure mitigation devices available, spoilers can be utilized along the roof lateral edges to suppress the formation of large vortices in that region (Li et al. [2]). The aerodynamic appendices can also be designed to reduce the wind loading on low-rise building roofs, which may be automatically adjusted according to instantaneous flow conditions. However, the feasibility of this load mitigation method depends on the spoiler dynamic stability and the strain/stress levels developed in the spoiler material.

In this sense, a fluid-structure interaction (FSI) model is proposed to numerically investigate the aeroelastic behavior and stress states induced by wind on aerodynamic appendages that are intended for future use in low-rise buildings to attenuate aerodynamic loading on roofs. In the present model, spoilers are considered elastic structures constituted of linear elastic material with geometrically nonlinear effects. The Finite Element Method (FEM) is adopted for spatial discretization using triangular shell elements (GPL_T9). The dynamic equilibrium

equation is integrated over time using the implicit Newmark algorithm and the α-generalized method. The system of flow equations consists of the Navier-Stokes equations and the mass conservation equation for incompressible and isothermal flows, while Large Eddy Simulation (LES) is employed for turbulence modeling using a dynamic sub-grid approach. The numerical formulation for flow analysis is based on a semi-implicit Characteristic-Based Split (CBS) model within the Finite Element Method framework, where linear tetrahedra are used for spatial discretization. Fluid-structure coupling is achieved using a partitioned model, incorporating an arbitrary lagrangean-eulerian (ALE) formulation for flow kinematics and a numerical scheme for mesh motion. Subcycling and techniques for transferring data across the fluid-structure interfaces are employed. The numerical formulation proposed here is validated using three-dimensional simulations based on wind tunnel tests referring to a typical low-rise building model.

2 Formulation

2.1 Flow equations

Some physical assumptions concerning the fluid flow modeling adopted here are initially presented (see, for instance, Braun and Awruch [3]): natural wind streams are considered to be within the incompressible and turbulent flow range; wind is constantly flowing with a constant temperature (isothermal process); gravity forces are neglected in the flow field; air is considered mechanically as a Newtonian fluid.

Consequently, the flow fundamental equations are reduced to the well-known Navier-Stokes and continuity equations, which are written here using an ALE kinematical description to consider the presence of moving bodies immersed in the flow field, while the flow turbulence is resolved using LES and Smagorinsky subgrid-scale modeling (Smagorinsky [4]; Germano et al. [5]; Lilly [6]) as follows:

$$\begin{aligned} &\frac{\partial v_i}{\partial t} + (v_j - w_j)\frac{\partial v_i}{\partial x_j} = \frac{1}{\rho}\frac{\partial}{\partial x_j}(\sigma_{ij} + \tau_{ij}^{SGS}) \qquad (i,j = 1,2,3) \qquad \text{in } \Omega^{\mathrm{f}}, \\ &\frac{\partial v_i}{\partial x_i} = 0 \qquad (i = 1,2,3) \qquad \text{in } \Omega^{\mathrm{f}}. \end{aligned} \tag{1}$$

In order to solve the flow problem, initial conditions on the flow variables v_i and p must be specified. In addition, appropriate boundary conditions must also be defined on $\Gamma_{\mathrm{t}}^{\mathrm{Tf}}$, which may be expressed as:

$$\begin{aligned} &v_i = w_i \qquad (i = 1,2,3) \qquad \text{on } \Gamma_{\mathrm{t}}^{\mathrm{fsi}}, \qquad v_i = \overline{v}_i \qquad (i = 1,2,3) \qquad \text{on } \Gamma^{\mathrm{v}}, \\ &p = \overline{p} \qquad \text{on } \Gamma^{\mathrm{p}}, \qquad \sigma_{ij} n_j = \left[-p\delta_{ij} + \tau_{ij}\right] n_j = t_i = \overline{t}_i \qquad (i,j = 1,2,3) \qquad \text{on } \Gamma^{\sigma}. \end{aligned} \tag{2}$$

where $\Gamma_{\mathrm{t}}^{\mathrm{fsi}}$ (boundary representing the fluid-structure interface), Γ^{v} (boundary with prescribed velocity $\overline{v}_i$), Γ^{p} (boundary with prescribed pressure $\overline{p}$) and Γ^{σ} (boundary with prescribed traction $\overline{t}_i$) are complementary subsets of $\Gamma_{\mathrm{t}}^{\mathrm{Tf}}$, such that $\Gamma_{\mathrm{t}}^{\mathrm{Tf}} = \Gamma_{\mathrm{t}}^{\mathrm{fsi}} \cup \Gamma^{\mathrm{v}} \cup \Gamma^{\mathrm{p}} \cup \Gamma^{\sigma}$. In Eq. (2), n_j are components of the unit normal vector **n** evaluated at a point on boundary Γ^{σ}. Notice that $w_i = 0$ is considered for points outside the ALE domain.

2.2 Flow numerical model

The Characteristic-based Split (CBS) scheme is formulated considering a coordinate shift along the flow characteristic directions to remove the advective term from the flow fundamental equations, which permits the use of standard Galerkin procedures in finite element spatial discretizations without the emergence of numerical instabilities. Mesh updating is avoided by using Taylor series approximations in the spatial domain and a split operation is utilized following a numerical procedure. The split operation enables the use of arbitrary interpolation functions for both the pressure and velocity fields and enhances pressure stability. Additional information on the CBS scheme may be found in Zienkiewicz et al. [7] and Nithiarasu et al. [8]. The standard Galerkin procedure is adopted here for spatial discretization of the flow equations after a temporal discretization operation is accomplished using the CBS scheme, where linear tetrahedral elements are utilized for both the velocity and pressure fields. Viscous and stabilizing terms are integrated by parts in steps 1 and 3, while the

pressure Laplacian is integrated by parts in step 2, leading to boundary terms. A system of linear algebraic equations is then obtained for the discretized flow equations, which are expressed in matrix form as:

Step 1: intermediate velocity

$$\tilde{\mathbf{v}}_i = \mathbf{v}_i^n - \mathbf{M}_d^{-1}\Delta t\left[\left(\mathbf{A}+\mathbf{D}\right)\mathbf{v}_i - \frac{\Delta t}{2}\mathbf{S}_v - \mathbf{f}_i\right]^n \qquad (i=1,2,3). \tag{3}$$

Step 2: pressure calculation

$$\mathbf{H}\mathbf{p}^{n+1} = \frac{\rho}{\Delta t}\mathbf{G}_i^T\tilde{\mathbf{v}}_i \qquad (i=1,2,3). \tag{4}$$

Step 3: velocity correction

$$\mathbf{v}_i^{n+1} = \tilde{\mathbf{v}}_i - \mathbf{M}_d^{-1}\frac{\Delta t}{\rho}\left[\mathbf{G}_i\mathbf{p}^{n+1} + \frac{\Delta t}{2}\left(\mathbf{S}_p\right)_i\mathbf{p}^n\right] \qquad (i=1,2,3). \tag{5}$$

where $\mathbf{v}_i$ and $\mathbf{w}_i$ are the flow and mesh velocity vectors evaluated at nodal level, $\mathbf{p}$ is the pressure nodal vector and $\mathbf{M}_d$ is the discrete mass matrix, which is obtained from the consistent mass matrix $\mathbf{M}$. A global time increment Δt is defined considering instantaneous flow conditions observed at element level (see Nithiarasu et al. [8]).

2.3 Algorithm for mesh movement

In FSI (Fluid-Structure Interaction) problems, the displacements or deformations of the structure can be considered in the fluid formulation through an Arbitrary Lagrangian-Eulerian (ALE) description. In this approach, the mesh in the ALE region must move according to a law that defines the mesh velocity field w_j in such a way that all elements maintain their integrity. Thus, a mesh movement scheme proposed by Teixeira [9] and adopted by Braun [10] is employed, in which the components of the mesh velocity vector are obtained as follows:

$$w_k^i = \frac{\sum_{j=1}^{Ns} a_{ij} w_k^j}{\sum_{j=1}^{Ns} a_{ij}} \qquad (k=1,2,3). \tag{6}$$

where Ns is the number of mesh points located on the boundaries of the ALE domain, and a_{ij} are the influence coefficients defined between mesh points i and j, where i refers to internal mesh points that are allowed to move, and j refers to mesh points on the boundary of the ALE domain, where w_j=0 . The influence coefficients a_{ij} are obtained by $a_{ij} = \left(d_{ij}\right)^{-n}$, with d_{ij} defining the Euclidean distance between mesh points i and j, and n is a user-defined parameter chosen according to the amplitude of the displacements of the immersed body, in order to avoid excessive mesh distortion. Typical values lie in range $1 \leq n \leq 4$.

2.4 Structure equations

The GPL-T9 finite element is used in this work to discretize the structure domain. First introduced by Zhang et al. [11] and later adopted by Teixeira [9], this element has proven to be both fast and accurate. The version employed here includes the in-plane drilling rotation Θ_{zi} of the midsurface, which prevents singularities in the stiffness matrix for coplanar elements and improves the numerical accuracy of the membrane variables. Each element has three nodes with six degrees of freedom per node (three displacement components and three rotational components). The total stiffness matrix is obtained by superimposing the membrane and bending stiffness matrices (Teixeira [9]). Further details of the formulation can be found in Zhang et al. [11].

The governing system of equations must account for geometric non-linearity and include inertia and

damping effects. Linearizing the dynamic equilibrium equation with the Newton–Raphson method yields the following global expression:

$$\mathbf{M}\ddot{\mathbf{u}}^{t+\Delta t} + \mathbf{C}\dot{\mathbf{u}}^{t+\Delta t} + \mathbf{K}^{t+\Delta t,i}\Delta\mathbf{u} = \mathbf{R}^{t+\Delta t} - \mathbf{F}^{t+\Delta t,i} \tag{7}$$

where $\mathbf{M}$ is the consistent mass matrix, built with linear shape functions equal for all translational degrees of freedom, $\mathbf{C}$ is the Rayleigh damping matrix, $\mathbf{K}^{t+\Delta t,i}$ is the tangent stiffness matrix at time $t + \Delta t$ and iteration i, comprising the linear and non-linear stiffness contributions, $\boldsymbol{R}^{t+\Delta t}$ is the external force vector at time $t + \Delta t$, $\mathbf{F}^{t+\Delta t,i}$ is the internal force vector at time $t + \Delta t$ and iteration i, while $\ddot{\mathbf{u}}$, $\dot{\mathbf{u}}$ and $\Delta\mathbf{u}$ are the nodal acceleration, velocity and displacement increment, respectively.

For the nonlinear dynamic analysis, the generalized-α method is adopted (see Braun [9] for additional information).

2.5 Algorithm for fluid–structure interaction analysis

In this work, a partitioned coupling scheme is adopted, in which the fluid flow and structural equations are solved independently and sequentially. Time integration is performed using a subcycling technique. For each time step taken by the structure, from t_n to t_{n+1}, the fluid is analyzed multiple times according to the subcycling factor:

$$n_{FE} = \Delta t_E \Big/ \Delta t_F \tag{8}$$

that is, the number of subcycles. As a result, the number of structural analyses is reduced, which in turn decreases the amount of data transfer across the fluid–structure interface. Once the specified number of subcycles is completed, the fluid solver provides the loads acting on the structure at the interface. The structure is then analyzed, supplying the fluid solver with the velocity field on the interface as boundary conditions for the next set of fluid subcycles.

3 Numerical examples

The numerical examples developed in this section are based on codes implemented in Fortran90, which were previously verified and validated in earlier studies for the fluid domain (Bianchin and Braun [1]) and for fluid-structure interaction (Bianchin and Braun [12]). Building on this foundation, the present study revisits the simulations presented by Bianchin and Braun [1], in which the action of spoilers—modeled as rigid bodies—was simulated to mitigate roof pressures on low-rise buildings. In that work, 28 tests were conducted considering a fixed spoiler to investigate the device's and to determine the optimal angle for maximum load mitigation under a specific wind incidence. Subsequently, a control law was implemented, allowing the device to rotate around its axis of rotation to the most effective aerodynamic position based on data collected by sensors located on the building's roof. Two- and three-dimensional simulations were performed to demonstrate that the mere attachment of the appendage already offers protection against strong wind gusts; however, when combined with control strategies and embedded technology, the system can provide even more favorable conditions for structural safety.

Thus, the development of this study begins with a two-dimensional fluid-structure interaction analysis (one element through the thickness), considering the same flow conditions, geometries, and meshes employed in previous works, incorporating spoilers modeled both as rigid bodies (non-deformable) and as deformable bodies with linear elastic material behavior. The finite element mesh used for the flow analysis consisted of 109,755 linear tetrahedral elements and 37,802 nodes, arranged in an unstructured manner. The physical properties of the flow are: density ρ = 1.2249 kg/m³, dynamic viscosity $\mu = 3.28 \times 10^{-4}$ Ns/m², characteristic velocity V = 30.0 m/s, characteristic length H = 1.25 m, Reynolds number Re = 1.4×10^5, Smagorinsky constant C_S = 0.1, and time step $\Delta t = 1 \times 10^{-4}$ s. Figure 1 presents the computational domain, geometry, and boundary conditions adopted here. The structure mesh was generated using triangular shell elements (50 elements and 52 nodes), positioned along the mid-thickness of the device and fully compatible with the fluid mesh. The structural properties, as defined in Gan et al. [13], are: density ρ_e = 192 kg/m³, Young's modulus $E = 9.76 \times 10^6$ N/m², Poisson's ratio v =

0.38, and the number of subcycles set to 10.

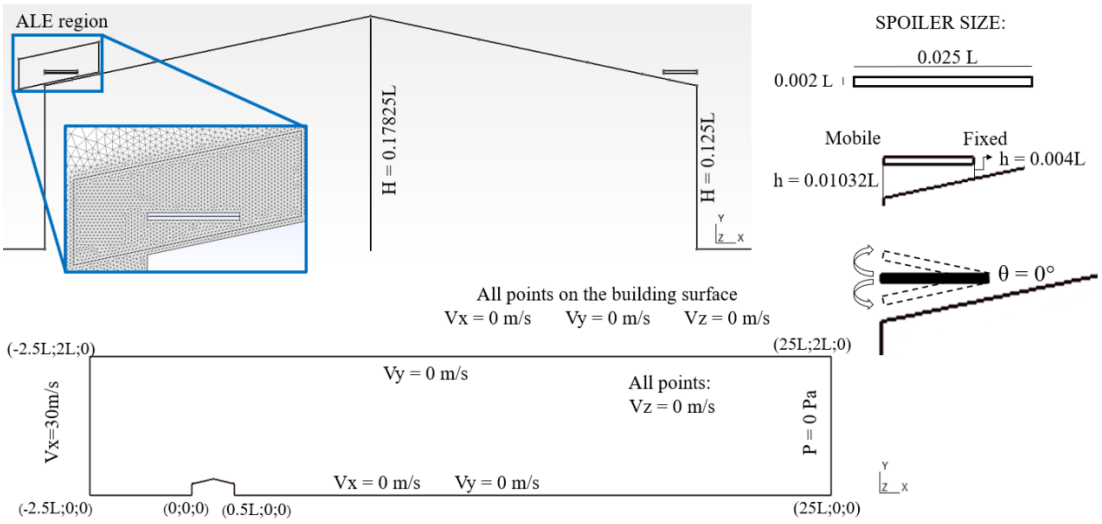
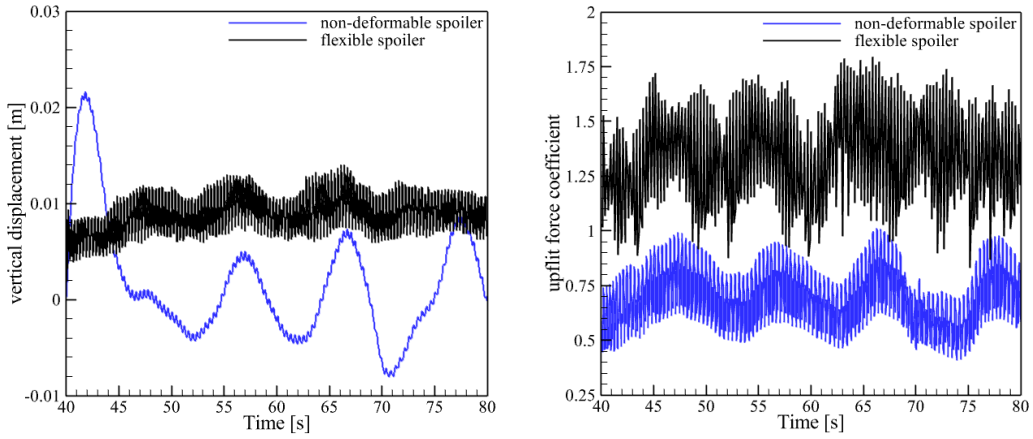


Figure 1. Geometric characteristics and boundary conditions

According to the descriptions above, two simulations under a 0° wind direction are analyzed in this section. In order to obtain consistent results, the flow field is first allowed to fully develop, with the spoilers considered as rigid and stationary. After 40 seconds, the structure is released to vibrate. To highlight the influence of spoiler vibration on the pressure field, the time histories of the vertical displacements at the spoiler's free end (Fig. 2a), the uplift force coefficient on the spoiler (Fig. 2b), and the uplift force coefficient on the windward roof of the building (Fig. 3) are presented.



(a) Vertical displacements at the spoiler's free end (b) Upflit coefficient on the spoiler

Figure 2. Time histories of structural response and upflit force on the spoiler

It is observed that the flexible spoiler (black line), which incorporates aeroelastic effects and exhibits lower structural stiffness, presents a higher vibration frequency and a lower displacement amplitude when compared to the non-deformable spoiler (Fig. 2a). On the other hand, the uplift coefficient is higher in the case of the flexible spoiler (Fig. 2b). This condition may indicate an underestimation of the forces acting on the device itself when it is considered non-deformable and highly rigid. Such a simplification can led to the neglect of relevant aeroelastic effects, which directly influence both the dynamic performance of the spoiler and the pressure distribution on the building roof. The uplift force coefficients obtained on the windward edge of the roof (Fig. 3), however, maintain similar amplitudes in both simulations, demonstrating the consistency of the numerical models and the effectiveness of both configurations in mitigating aerodynamic pressure effects.

Figures 4a, 4b, and 4c show the pressure fields obtained at 60 seconds of simulation, considering,

respectively, the building without a spoiler, with a non-deformable spoiler, and with a flexible spoiler. The qualitative results confirm the expected behavior: the effectiveness of the spoilers in deflecting vortices away from the building roof, indicating the feasibility of their use as an aerodynamically efficient and safe system. Additionally, Figure 4c highlights the presence of high pressure acting on the flexible spoiler, with the resulting deformation effects shown in Figure 4d. From these visualizations, it can be observed that the aeroelastic effects lead to a reduced oscillatory motion of the device, which tends to adopt a parabolic shape as a result of its lower structural stiffness. In both scenarios, the spoilers effectively deflect the roof-edge vortices, altering the flow pattern in the region of the roof most susceptible to high suction pressures.

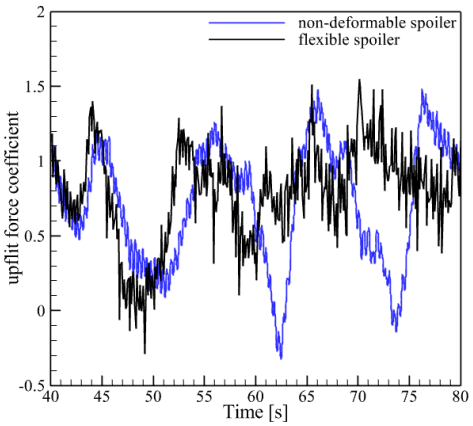


Figure 3. Uplift force coefficient on the windward roof

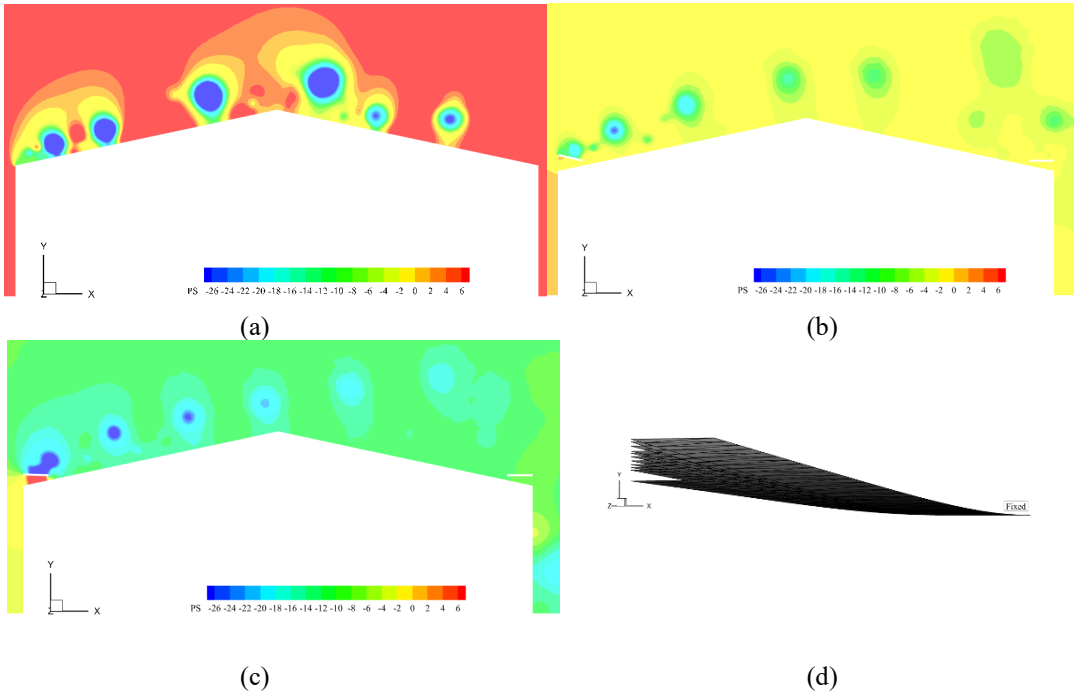


Figure 4. Pressure field in 60s for: (a) spoiler-free building; (b) building with non-deformable spoiler; (c) building with flexible spoiler, and (d) deformations of the flexible spoiler

4 Conclusions

Two-dimensional fluid-structure interaction (FSI) simulations were conducted to analyze how the aeroelastic and rigid behaviors of spoilers influence wind pressure on buildings. The results indicate that the force acting on the spoiler is significantly increased when the aeroelastic effects are considered. In addition, it is

observed that the vertical displacements obtained at the spoiler's free with the aerolastic model presents a higher averaged displacement, although presenting smaller amplitudes, when compared with the predictions obtained with the non-deformable model. On the other hand, the load on the roof remains practically the same when the spoiler is modeled using the aeroelastic and rigid body approaches.

Wind tunnel testing methods and CFD approaches recommended by most current design codes are generally based on rigid structural models. However, as demonstrated by the numerical results of Gan et al. [13], these methods may underestimate the actual negative wind pressure in buildings equipped with spoilers. For a more accurate assessment of wind loads, especially in the presence of spoilers, it is essential to consider aeroelastic effects through FSI simulations and dedicated aeroelastic experiments. During the spoiler design process, it is recommended to increase its structural stiffness whenever possible to allow for more appropriate rotation and to minimize displacements at the center of the device.

Finally, three-dimensional simulations are recommended to better understand the aeroelastic effects along the width of the spoiler and their consequences for the roof.

Acknowledgements. The authors would like to thank the National Council for Scientific and Technological Development (CNPq, Brazil) and the Brazilian Federal Agency for Support and Evaluation of Graduate Education (CAPES, Brazil) for the financial support.

Authorship statement. The authors hereby confirm that they are the sole liable persons responsible for the authorship of this work, and that all material that has been herein included as part of the present paper is either the property (and authorship) of the authors or has the permission of the owners to be included here.

References

[1] G. P. Bianchin, A. L. Braun, "Numerical investigation on wind pressure mitigation in low-rise building roofs using spoilers with PID control". In: Latin American Journal of Solids and Structures, v. 22, n. 1, p. e8383, 2025.
[2] G. Li, S. Gan, H. Li, "Wind pressure mitigation on gable roofs for low-rise buildings using spoilers", In: Journal of Structural Engineering – ASCE 144(8) (2018) 1–14.
[3] A.L. Braun, A.M. Awruch, Aerodynamic and aeroelastic analyses on the CAARC standard tall building model using numerical simulation, Computers and Structures 87(9-10) (2009) 564-581.
[4] J. Smagorinsky, General circulation experiments with the primitive equations, I, the basic experiment, Monthly Weather Review 91 (1963) 99-135.
[5] M. Germano, U. Piomelli, P. Moin, W.H. Cabot, A dynamic subgrid-scale eddy viscosity model, Physics of Fluids 3 (1991) 1760-1765.
[6] D.K. Lilly, A proposed modification of the Germano subgrid-scale closure method, Physics of Fluids 4 (1992) 633-635.
[7] O.C. Zienkiewicz, R.L. Taylor, P. Nithiarasu, The Finite Element Method for Fluid Dynamics, 7th ed., Butterworth-Heinemann, Waltham, 2013.
[8] P. Nithiarasu, R.W. Lewis, K.N. Seetharamu, Fundamentals of the Finite Element Method for Heat and Mass Transfer, 2nd ed., Wiley, Chichester, West Sussex, 2016.
[9] P. R. d. F. Teixeira, "Simulação numérica da interaçao de escoamentos tridimensionais de fluídos compressíveis e incompressíveis e estruturas deformáveis usando o Método dos Elementos Finitos", Tese de Doutorado, Universidade Federal do Rio Grande do Sul, Porto Alegre, 2001.
[10] A. L. Braun, "Simulação numérica na engenharia do vento incluindo efeitos de interação fluido-estrutura.", Tese de Doutorado, Universidade Federal do Rio Grande do Sul, Porto Alegre, 2007.
[11] Q. Zhang, L. Mu e K. Wenqi, "Geometric non-linear analysis of space shell structures using generalized conforming flat shell elements – for space shell structures", Communications in numerical methods in engineering, v. 14, n. 11-14, pp. 941–957, 1998. doi: https://doi.org/10.1016/j.compstruc.2007.01.025.
[12] G. P Bianchin, A. L. Braun, "Modelo de Interação Fluido-Estrutura utilizando método Characteristic-Based Split (CBS) com elementos de casca GPL-T9 e metodologia Large Eddy Simulation (LES). XII ERMAC, Porto Alegre, 2025.
[13] S. Gan, G. Li, Z. Dong, H. Li, M Zhao, "Numerical study on aeroelastic behavouir of spoiler on low-rise building based on fluid-structure interaction method.", Journal od building engineering, vol. 59, 2022. https://doi.org/10.1016/j.jobe.2022.105115